

## Effect of $K_2CO_3$ additive on crystallinity and piezoelectric properties of KNNS-BZ-BKH ceramics

Lihaowen Zeng<sup>a</sup>, Rabie Benioub<sup>a</sup> and Kenji Itaka<sup>b,\*</sup>

<sup>a</sup>Graduate School of Science and Technology, Hirosaki University, 1 Bunkyo-cho, Hirosaki, Aomori, 036-8560, Japan

<sup>b</sup>Institute of Regional Innovation, Hirosaki University, 2-1-3, Matsubara, Aomori, 030-0813, Japan

In this study, the piezoelectric ceramics,  $(0.955) K_{0.48}Na_{0.52}Nb_{0.9}Sb_{0.1}O_3-(0.025) BaZrO_3-(0.02) Bi_{0.5}K_{0.5}HfO_3$  (KNNS-BZ-BKH) with  $m$  mol%  $K_2CO_3$  additives in the range of  $m = 0.0$  to 3.96 have been successfully fabricated using the solid-state reaction method. The effect of  $K_2CO_3$  on the sintering behavior, structure, microstructure, and electrical properties of KNNS-BZ-BKH ceramics was investigated. The experimental results showed that the addition of  $K_2CO_3$  improved the sintering process of KNNS-BZ-BKH, which exhibited a well-sintered ceramic with a dense and pure perovskite structure stoichiometrically. At an optimal sintering temperature of 1210 °C and  $K_2CO_3$  content of 2.64 mol%, enhanced physical properties of the ceramics such as density 4.0 g cm<sup>-3</sup> and piezoelectric constant  $d_{33} = 75$  pC/N were obtained through enhancement of KNNS-BZ-BKH microstructures with the best results exhibiting a pure perovskite phase with no secondary phases due to crystallinity improvement.

**Keywords:** KNN-based, Ceramics, Crystallinity, Piezoelectric, Lead-free.

### Introduction

Piezoelectric materials are enablers of conversion between mechanical and electrical energy in both directions through transducer elements from ignitors, actuators, and sound generators to filters and sensors [1-4]. Lead-based ceramics such as  $Pb(Zr,Ti)O_3$  (PZT) dominated the piezoelectric materials market for electronics and energy industry applications in the last century because of their excellent properties and flexibility in terms of compositional modification [5-9]. However, due to their harmful nature, the appearance of new regulations, and the expansion of Restriction of Hazardous Substances of the European Union (RoHS), the development of lead-free materials with the same level attracted much attention [10-14]. Alkali niobate system (K, Na)  $NbO_3$  abbreviated (KNN-based) materials have been considered one of the most promising candidates to replace lead-based piezoelectric materials, among the other alternative replacements due to their excellent piezoelectric constant ( $d_{33}$ ), high Curie temperature, and their good comprehensive performance [15-19]. Saito et al. reported an impressive  $d_{33}$  of over 400 pC/N for Sb-introduced KNN grown by reactive-template grain growth [20]. Furthermore, the KNN-based ceramics piezoelectric response highly depends on temperature due to their polymorphic phase boundaries (PPB) instead of morphotropic phase

boundaries (MPB) characterizing PZT-based materials [21-27]. In order to overcome this problem, the addition of various materials improved temperature stability by shifting the corresponding  $T_{O-T}$  (orthorhombic-tetragonal) below room temperature [28-29]. The effect of various additives on the phase transition temperatures and electrical properties in the series of KNN-based ceramics were investigated [30], such as  $Bi_{0.5}A_{0.5}ZrO_3$  ( $A = K, Na, Ag$ ) [31],  $(Li, K, Na)(Nb, Sb)O_3-(Bi, Na, Sr)ZrO_3$  with dopants  $CuO, B_2O_3, ZnO$  [32],  $(K, Na)(Nb, Cu)O_3-SrZrO_3$  [33], and  $(Na, Bi)TiO_3-(Ba, Ca)(Ti, Zr)O_3-(K, Na)NbO_3$  [34]. Xu et al. reported a giant  $d_{33}$  of ~570 pC/N using  $Sb^{5+}$ ,  $BaZrO_3$ , and  $Bi_{0.5}K_{0.5}HfO_3$  (KNNS-BZ-BKH) as additives to shift their  $T_{R-O}$  (rhombohedral-orthorhombic) as well as  $T_{O-T}$  to or near room temperature fabricated by the conventional solid-state method [35].

Moreover, the conventional solid-state sintering process results illustrated difficulties of the process for KNN-based dense ceramics [36]. Various research works on substitute methods that enhance the density of the fabricated KNN ceramics have been conducted, such as plasma [37], hot temperature processing [38], and recently two-step sintering method, which is showing high efficiency for the enhanced piezoelectric properties on the KNN-based ceramics [39]. However, due to the lack of a clear understanding of the relationship between the sintering temperature and the crystallinity of KNN-based ceramics and their impact on the piezoelectric constant ( $d_{33}$ ) at room temperature, it is mandatory and inevitable to elucidate the different aspects of the

\*Corresponding author:  
Tel : +81-17-762-7760  
Fax: +81-17-735-5411  
E-mail: itaka@hirosaki-u.ac.jp

modified sintering process effect on both KNN-based microstructures and piezoelectric properties.

In this work, we investigated the effect of sintering temperature and  $K_2CO_3$  as additives on the crystallinity and piezoelectric properties of  $0.955K_{0.48}Na_{0.52}Nb_{0.9}Sb_{0.1}O_3-0.025BaZrO_3-0.02Bi_{0.5}K_{0.5}HfO_3$  (abbreviated as KNNS-BZ-BKH) ceramics. The crystallinity dependency on the sintering temperature and the  $K^+$  additive content, in addition to the resultant piezoelectric properties of KNNS-BZ-BKH sintered at 850 °C and 1210 °C, are discussed in terms of microstructures and formation defects.

## Experimental

The KNNS-BZ-BKH +  $m$   $K_2CO_3$  piezoelectric ceramics, where  $m = 0.0, 0.66, 1.32, 1.98, 2.64, 3.30$  and  $3.96$  mol%, that is, approximately  $m = 0, 0.5, 1, 1.5, 2, 2.5$  and  $3$  wt%, were synthesized by a conventional solid-state reaction method. In order to prepare the KNNS-BZ-BKH piezoelectric materials, 99.9% raw reagent-grade of  $Bi_{0.5}K_{0.5}HfO_3$ ,  $BaZrO_3$ ,  $K_{0.48}Na_{0.52}Nb_{0.9}Sb_{0.1}O_3$ , and  $K_2CO_3$  were used as starting materials. Firstly, the materials were weighed, mixed according to their stoichiometric composition, and milled with the appropriate volume of ethanol in a planetary micro ball mill (Pulverisette) for 24 h with Agate balls. After dry up the ethanol, the powders were calcined at 850 °C, 1100 °C, and 1210 °C for 6 h to compare the effect of calcination temperature on the crystallinity of KNNS-BZ-BKH shown in Fig. 1(a). Then the calcined powders with 850 °C were processed by polyvinyl alcohol (PVA) into compacted disks with diameters of 10 mm and thickness of 1~2 mm. After the PVA was burned off, the pellets were sintered at 1090~1210 °C for 6 h. Silver electrodes on both sides of the sintered pellets were made with silver paint (DuPont, #4922) and polarized under a direct current electric field of 13~18 kV/cm in a silicone oil bath at 50-100 °C for 10-120 min as shown in Fig. 1(b).

The structural properties of the calcined powder with various temperatures and with different K additives were characterized using x-ray diffraction (XRD) with a Cu-K $\alpha$  ( $\lambda = 0.15405$  nm) radiation source in the angular range of  $20^\circ \leq 2\theta \leq 90^\circ$  and at a scan rate of  $10^\circ/\text{min}$  was employed by an x-ray diffractometer (Smartlab, Rigaku Corporation). Full Width at Half Maximum (FWHM) was determined by Voigt function

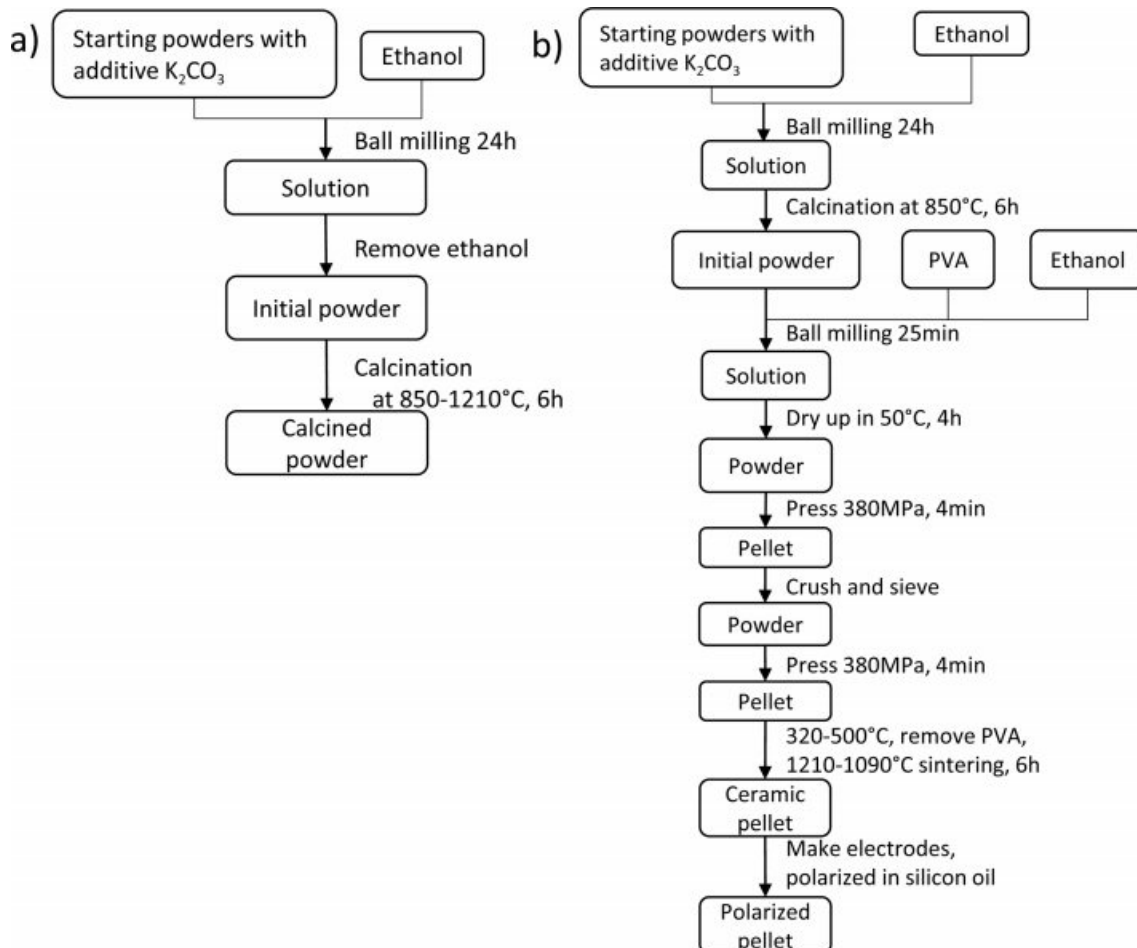


**Fig. 1.** Flow chart of the fabrication process for (a) powder samples and (b) pellet samples.

fitting. A scanning electron microscope (SEM, Hitachi SU8010) equipped with an energy dispersive spectrometer (EDS, HORIBA Scientific) analyzer was used for microstructure and composition analysis. The oxygen component was excluded in the estimation to remove the effect on the other elements due to the significant error of EDS peaks on the light element. The piezoelectric properties were measured using Piezoelectric Constant ( $d_{33}$ ) Calibrator (YE2730A, SINOCERA PIEZOTRONICS INC.).

## Results and Discussion

Fig. 2(a) shows the powder XRD patterns of the KNNS-BZ-BKH powder prepared without  $K_2CO_3$  additive (*i.e.*,  $m = 0$ ) measured after the following heat treatments: (T1) just after heat treatment at 150 °C for 3 h for ethanol removal, (T2) firstly, calcination at 850 °C for 6 h, (T3) two-step calcination of firstly at 850 °C for 6 h, and secondly at 1100 °C for 6 h, and (T4) two-step calcination of firstly with 850 °C for 6 h and secondly temperature profile with gradually change from 1210 °C to 1090 °C for 6 h. A perovskite structure without a secondary phase was observed for calcined heating patterns of (T3) and (T4). The unreacted raw material peaks as secondary phases in the case of (T1) and (T2) were observed at  $2\theta = 22^\circ$  (corresponding to KNNS), at  $2\theta = 30^\circ, 43^\circ,$  and  $54^\circ$  ( $BaZrO_3$ ), at  $2\theta = 47^\circ$  and  $64^\circ$  ( $Bi_{0.5}K_{0.5}HfO_3$ ). Fig. 2(b) shows the enlarged peaks of (110) in the  $2\theta$  range of  $31^\circ$  to  $33^\circ$ . Broad (110) peaks in only the cases of (T1) and (T2) were observed (FWHM of (T1) =  $0.461^\circ$ , FWHM of (T2) =  $0.403^\circ$ ), while sharp (110) peaks in the case of (T3) and (T4) were observed (FWHM of (T3) =  $0.341^\circ$ , FWHM of (T4) =  $0.251^\circ$ ). The (110) peaks moved towards higher angles due to the formation of the KNNS-BZ-BKH perovskite structure. In additional experiments,

we found that the secondary heating at a fixed temperature of 1210 °C causes the decomposition of the samples. So, we could conclude that the calcination process with (T4) temperature profile was optimal in the viewpoint of the crystallinity and endorsed the formation of perovskite structure based on the XRD results obtained for KNNS-BZ-BKH powder calcination.

Fast forward, we focused on the study of the effect of adding various molar ratios of  $K_2CO_3$ . Fig. 3 shows estimated potassium mol% (except oxygen) by SEM/EDS as a function of additive  $K_2CO_3$  ( $m$  mol%). The estimated potassium increased linearly in the range of 22 to 25 mol% with varying  $m$ . This result shows the stoichiometric component for K around 1.98 mol% as optimal. Table 1 shows the molar ratios of Na, Zr, Nb,

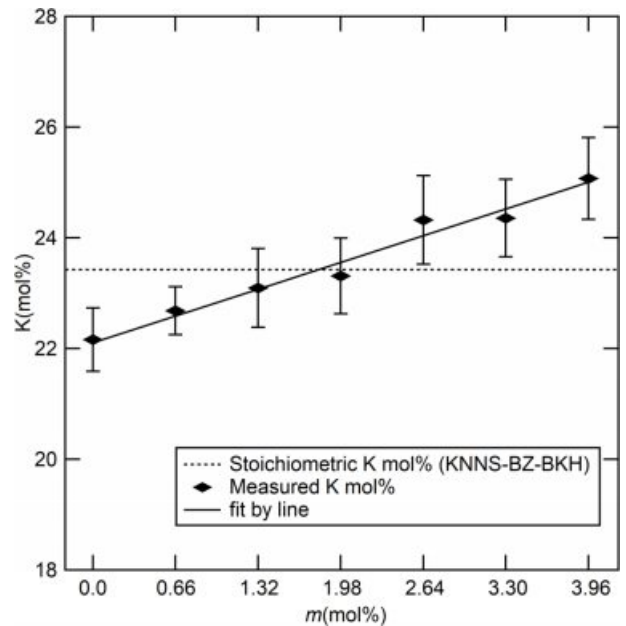


Fig. 3. The molar ratio (mol%) of potassium K with additive  $m$ .

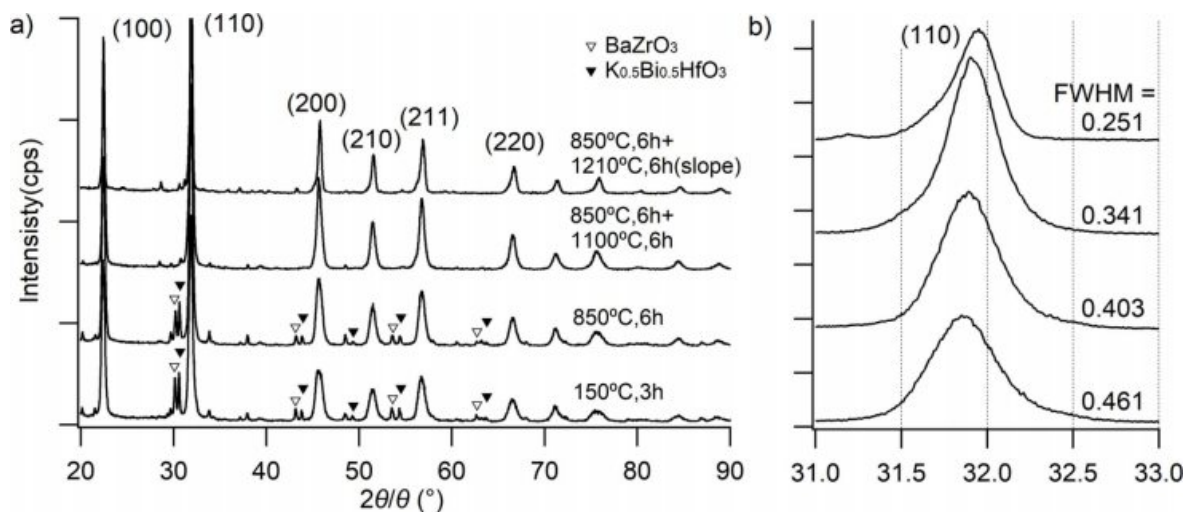


Fig. 2. XRD patterns of powder under different heating patterns ( $m = 0$ ): (a) the XRD pattern between  $20^\circ$  and  $90^\circ$ ; (b) the XRD pattern between  $31^\circ$  and  $33^\circ$ .

**Table 1.** The molar ratios (mol%) of Na, Zr, Nb, Ba, Hf, and Bi, estimated by EDS analysis and calculated by starting compositions as a function of  $K_2CO_3$  additives ( $m$  mol%)

$m$		K	Na	Zr	Nb	Sb	Ba	Hf	Bi
0	designed	23.42	24.83	1.25	42.98	4.78	1.25	1.00	0.50
	measured	22.16	22.83	1.34	44.47	5.11	1.41	1.84	0.84
0.66	designed	23.92	24.67	1.24	42.69	4.74	1.24	0.99	0.50
	measured	22.68	23.02	1.01	44.20	5.05	1.39	1.79	0.85
1.32	designed	24.42	24.51	1.23	42.42	4.71	1.23	0.99	0.49
	measured	23.09	22.39	1.26	44.73	4.80	1.39	1.63	0.72
1.98	designed	24.91	24.35	1.23	42.14	4.68	1.23	0.98	0.49
	measured	23.31	22.08	0.95	45.11	4.81	1.41	1.73	0.60
2.64	designed	25.39	24.19	1.22	41.87	4.65	1.22	0.97	0.49
	measured	24.32	21.39	1.36	44.75	4.52	1.23	1.73	0.69
3.30	designed	25.87	24.04	1.21	41.60	4.62	1.21	0.97	0.48
	measured	24.35	22.00	1.39	44.08	4.71	1.35	1.56	0.56
3.96	designed	26.34	23.88	1.20	41.34	4.59	1.20	0.96	0.48
	measured	25.07	20.94	1.29	44.30	4.72	1.46	1.57	0.64

Ba, Hf, and Bi (mol%) estimated by EDS analysis and calculated by starting compositions as a function of  $K_2CO_3$  additives ( $m$  mol%). In the case of  $m = 0$ , the molar ratio of each element is approximately consistent in the estimation and the calculation. However, the

molar ratio of K is relatively lower as compared with other elements. Therefore, the  $K_2CO_3$  additive is effective in compensating for the lack of potassium. All elements except K were approximately independent of the  $K_2CO_3$  additives.

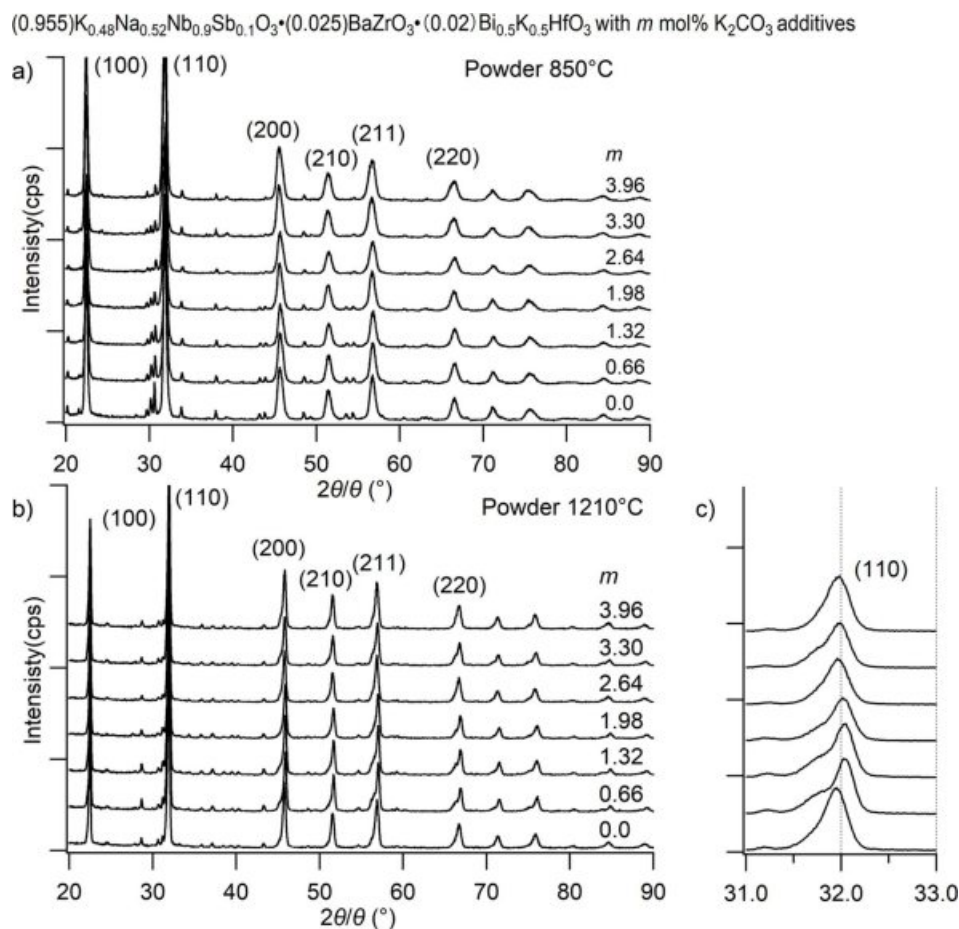
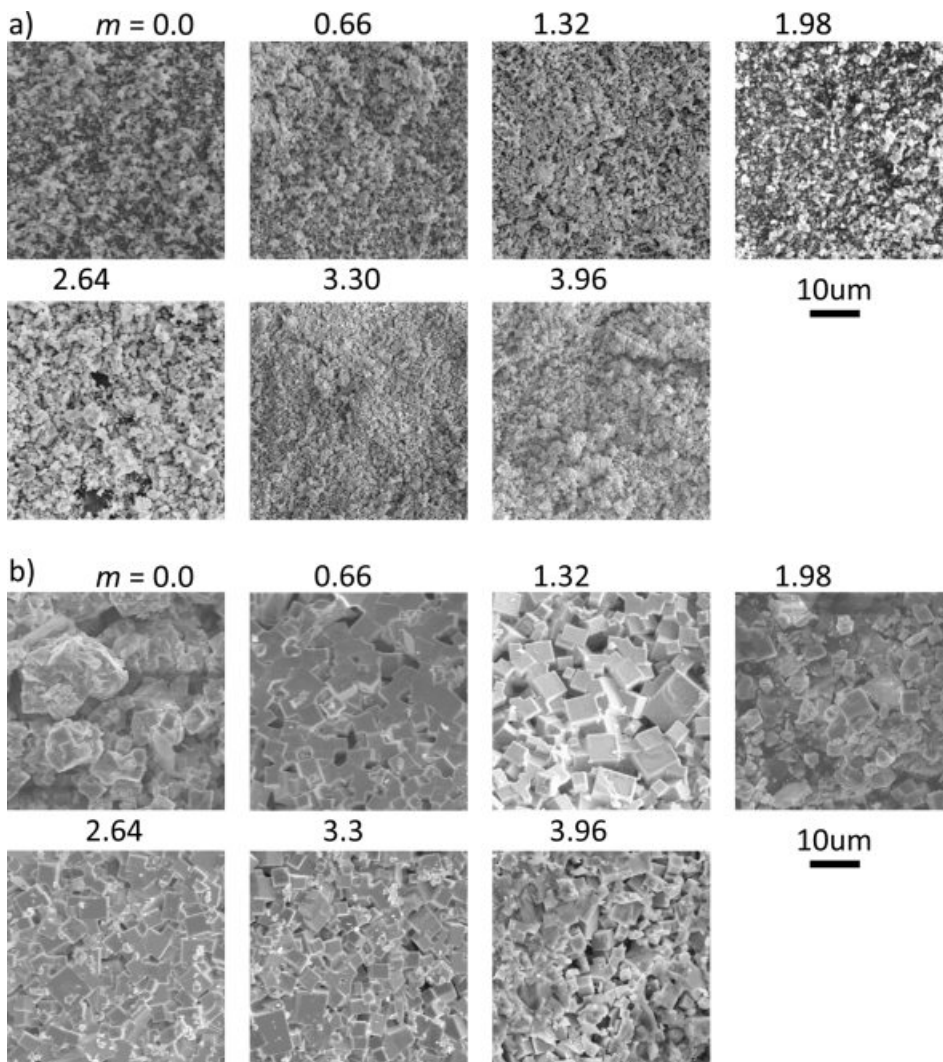
**Fig. 4.** XRD patterns of powder with different  $m$  (a) samples after 850 °C heating (b) (c) samples after 1210 °C heating.

Fig. 4 shows XRD diffractions patterns corresponding to KNNS-BZ-BKH ceramics powder doped with different  $K_2CO_3$  amounts (0 to 3.96 mol%) and calcined with (T2) temperature profile (850 °C) in Fig. 4(a) and (T4) temperature profile (1210 °C) in Fig. 4(b). The presence of a predominant phase related to KNNS with a main orthorhombic perovskite structure has been detected. Small peaks associated with the presence of a secondary phase can be assigned to partially unreacted powder mixture or impurities when calcined under (T2) condition and decreasing with an increase in  $K_2CO_3$  additives ( $m$  mol%). In the case of the calcination under (T4) condition, Fig. 4(b) shows a significant decrease in impurity phases even at  $m = 0$ . In contrast, a more decrease in impurity phases is shown with an increase in  $m$  led to further suppression of secondary phases. The precise evaluation of the  $K_2CO_3$   $m$  mol% additive effect on the crystallinity of KNNS-BZ-BKH ceramics, Fig. 4(c) shows an XRD diffraction peak corresponding to (110) at  $2\theta = 31.8^\circ$  for KNNS-BZ-BKH powder calcined with (T4) condition. The location of (110) peak increased

from  $m = 0$  to 1.98~2.64 mol%, which corresponds to the stoichiometry of K mol% value as shown in Fig. 3. While, the increase in the additive  $m$  over 2.64 mol% led the location of (110) peak to decrease slightly towards lower angles due to excess of  $K_2CO_3$  additives, as shown in Fig. 3.

These results showed that  $K_2CO_3$   $m$  mol% additive has an optimal range of 1.98~2.64 mol% in which KNNS-BZ-BKH crystallinity is enhanced via impurity phases removal or entirely reaction of mixture led to the appearance of perovskite structure without secondary phases induced by unreacted raw materials due to highly volatile K element during sintering process with (T4) condition. The diffraction peaks shift toward a higher angle with increasing  $K_2CO_3$  addition since it is expected that  $K^+$  (0.164 nm) could substitute for  $Bi^{3+}$  (0.14 nm) and  $Na^+$  (0.139 nm). Only an orthorhombic phase with a perovskite structure was observed. It indicates that the addition of small amounts of  $K_2CO_3$  (0~3 wt%) did not give rise to an apparent change in the crystal structure.



**Fig. 5.** SEM pictures (2000 magnification) of powder with different  $m$  (a) samples after 850 °C heating (b) samples after 1210 °C heating.

Fig. 5 shows the SEM images of the KNNS-BZ-BKH with 0~3.96 mol%  $K_2CO_3$  additives, ceramics sintered with (T2) temperature profile (850 °C) in Fig. 5(a) and (T4) temperature profile (1210 °C) in Fig. 5(b). The pure KNNS-BZ-BKH ceramic powder sintered with (T2) temperature profile exhibited a small grain size (200-300 nm), and no noticeable change in the morphology of the specimen occurred even with various amounts of  $K_2CO_3$  additive. On the other hand, in the case of the (T4) temperature profile, the facets based on the crystal structure were observed. The microstructure in which abnormal grains larger than 700 nm and average grains of 300 to 700 nm coexisted was observed with dense microstructure due to overall grain growth. The most apparent facets were observed at  $m = 1.32$ , but the gaps between the grains were rather large. It seems that additives with  $m = 1.98$  to 3.3 show denser morphology, with facets being nucleated. This change in the grain gap may be correlated with the change in the (110) peak shown in Fig. 4(c).

Table 2 shows the specimens' bulk density and piezoelectric properties sintered with (T4) temperature profile (1210 °C). We faced difficulty forming the pellet and polarization due to the following reasons in our current process: (1) the pellet in the alumina crucible melted and stuck to the alumina crucible. (2) the pellet was broken into pieces during the polishing process due to the fragile and sparse pellets. (3) the pellet could not be polarized enough due to the leak current between the electrodes. Due to these difficulties of the palletization and polarization process, the  $m = 0.66$  mol% and 1.32 mol% samples could not be made into well-polarized pellets. Here, we investigated only the successfully made pellet according to the amount of  $K_2CO_3$  additive ( $m = 0, 1.98, 2.64, 3.3, \text{ and } 3.96$  mol%).

The measured density of KNNS-BZ-BKH ceramics as a function of  $K_2CO_3$  addition slightly increases with increasing  $K_2CO_3$  additives. The piezoelectric charge coefficient ( $d_{33}$ ) of pure KNNS-BZ-BKH ceramic without additive was 35.5 pC/N while adding  $K_2CO_3$   $m = 1.98$  mol% led to a decrease of  $d_{33}$  value to almost half 18.5 pC/N despite exhibiting a better crystallinity in Fig. 4. Nevertheless,  $d_{33}$  increased with additive  $m = 2.64$  mol% to 75 pC/N, consistent with the XRD diffraction patterns for powder in Fig. 4(c) and SEM images exhibiting higher grain growth in Fig. 5(b). The  $d_{33}$  values of the ceramics with additive over  $m = 2.64$

mol% exhibited a sharp decrease due to excess of  $K_2CO_3$  additive leading to poor crystallinity and smaller grains. The sample size of the crystal and the gaps between the grains observed in SEM images of Fig 5(b) seem to influence the piezoelectric properties strongly. All the pellets showed almost the same density, and the dielectric constant and dielectric loss did not change significantly except for  $m = 3.3$  mol% pellets. The pellet of  $m = 3.3$  mol% may have an unknown problem in our pelletizing process.

## Conclusion

The adding  $K_2CO_3$  in the range of 0~3.96 mol% (3 wt%) on KNNS-BZ-BKH ceramics maintained the structure of the orthorhombic phase of perovskite. Calcination temperature at 1210 °C played a significant role in enhancing the crystallinity of the mixed KNNS-BZ-BKH by improving the reaction rate between main KNNS and secondary phases  $BaZrO_3$  and  $(Bi, K)HfO_3$ . An optimum range for higher KNNS-BZ-BKH crystallinity is achieved via calcination temperature at 1210 °C combined with  $K_2CO_3$  additive 1.98~2.64 mol%. The highest piezoelectric constant  $d_{33}$  value of 75 pC/N was observed at the optimum additive range. The addition of easily evaporated elements such as potassium compared with the stoichiometric ratio was shown to be effective in improving crystallinity and piezoelectric properties.

## Acknowledgment

We gratefully thank Mr. Hiroshi Komiya (MICRONICS JAPAN Co., Ltd.) for valuable discussions and advice. This work was partially supported by JSPS KAKENHI Grant Number 20K05178. We gratefully acknowledge support from the Rotary Yoneyama Memorial Foundation.

## References

1. T. Zheng, J.G. Wu, D.Q. Xiao, and J.G. Zhu, Prog. Mater. Sci. 98 (2018) 552-624.
2. H.C. Thong, C.L. Zhao, Z. Zhou, C.F. Wu, Y.X. Liu, Z.Z. Du, J.F. Li, W. Gong, and K. Wang, Mater. Today 29 (2019) 37-48.
3. Z.Y. Cen, X.H. Wang, Y. Huan, and L.T. Li, J. Am. Ceram. Soc. 101[6] (2018) 2391-2407.
4. K.H. Cho, B.G. Choi, B.G. Loh, Z.S. Lim, D.H. Kim, B.J. Ko, Y.H. Kim, S.M. Kim and K.B. Shim, J. Ceram. Process. Res. 12[5] (2011) 610-614.
5. J. Rödel and J.F. Li, MRS Bull. 43[8] (2018) 576-580.
6. J.G. Hao, W. Li, J.W. Zhai, and H. Chen, Mater. Sci. Eng. R-Rep. 135 (2019) 1-57.
7. P. Li, X.Q. Chen, F.F. Wang, B. Shen, J.W. Zhai, S.J. Zhang, and Z.Y. Zhou, ACS Appl. Mater. Interfaces 10[34] (2018) 28772-28779.
8. C.L. Zhao, B. Wu, K. Wang, J.F. Li, D.Q. Xiao, J.G. Zhu, and J.G. Wu, J. Mater. Chem. A 6[46] (2018) 23736-23745.

**Table 2.** Comparison of the properties of 0.955KNNS-0.025BZ-0.02BKH with different  $m$  mol% of additives  $K_2CO_3$

$m$ (mol%)	0	1.98	2.64	3.30	3.96
$d_{33}$ (pC/N)	35.5	18.5	75	47	31.5
$\epsilon_r$	229	286	181	443	257
$\tan \delta$	0.055	0.055	0.058	0.029	0.042
Density (g/cm <sup>3</sup> )	4.0±0.1	3.9±0.3	4.0±0.3	4.1±0.3	4.1±0.3

9. G.Y. Lee, D. Cho, M. Jeong, and C.S. Lee, *J. Ceram. Process. Res.* 10[4] (2009) 526-528.
10. Y. Quan, W. Ren, G. Niu, L.Y. Wang, J.Y. Zhao, N. Zhang, M. Liu, Z.G. Ye, L.Q. Liu, and T. Karaki, *ACS Appl. Mater. Interfaces* 10[12] (2018) 10220-10226.
11. P. Li, Y. Huan, W.W. Yang, F.Y. Zhu, X.L. Li, X.M. Zhang, B. Shen, and J.W. Zhai, *Acta Mater.* 165 (2019) 486-495.
12. X. Lv, J.G. Wu, J.G. Zhu, and D.Q. Xiao, *Phys. Chem. Chem. Phys.* 20[30] (2018) 20149-20159.
13. X. Lv, J.G. Wu, C.L. Zhao, D.Q. Xiao, J.G. Zhu, Z.H. Zhang, C.H. Zhang, and X.X. Zhang, *J. Eur. Ceram. Soc.* 39[2-3] (2019) 305-315.
14. S.H. Lee, S.P. Nam, S.G. Lee, S.C. Lee, and Y.H. Lee, *J. Ceram. Process. Res.* 12[3] (2011) 332-335.
15. J. Wang and L.H. Luo, *J. Am. Ceram. Soc.* 101[1] (2018) 400-407.
16. Q. Liu, Y.C. Zhang, J. Gao, Z. Zhou, H. Wang, K. Wang, X.W. Zhang, L.T. Li, and J.F. Li, *Energy Environ. Sci.* 11[12] (2018) 3531-3539.
17. S. Trolrier-McKinstry, S.J. Zhang, A.J. Bell, and X.L. Tan, *Ann. Rev. Mater. Res.* 48 (2018) 191-217.
18. X. Lv, Z.Y. Li, J.G. Wu, D.Q. Xiao, and J.G. Zhu, *ACS Appl. Mater. Interfaces* 8[44] (2016) 30304-30311.
19. A.L. Ding and H.F. Wang, *J. Ceram. Process. Res.* 11[1] (2010) 44-46.
20. Y. Saito, H. Takao, T. Tani, T. Nonoyama, K. Takatori, T. Homma, T. Nagaya, and M. Nakamura, *Nature* 432[7013] (2004) 84-87.
21. D.K. Liu, X.C. Zhang, W.B. Su, X.M. Wang, W.Z. Yao, C.M. Zhou, and J.L. Zhang, *J. Alloy. Compd.* 779 (2019) 800-804.
22. Q. Li, M.H. Zhang, Z.X. Zhu, K. Wang, J.S. Zhou, F.Z. Yao, and J.F. Li, *J. Mater. Chem. C* 5[3] (2017) 549-556.
23. H. Tao, H.J. Wu, Y. Liu, Y. Zhang, J.G. Wu, F. Li, X. Lyu, C.L. Zhao, D.Q. Xiao, J.G. Zhu, and S.J. Pennycook, *J. Am. Chem. Soc.* 141[35] (2019) 13987-13994.
24. N. Zhang, T. Zheng, C.L. Zhao, X.W. Wei, and J.G. Wu, *J. Mater. Res.* 36[5] (2021) 1142-1152.
25. X. Lv, J.G. Wu, D.Q. Xiao, J.G. Zhu, and X.X. Zhang, *Acta Mater.* 140 (2017) 79-86.
26. K. Wang, B. Malič, and J.G. Wu, *MRS Bull.* 43[8] (2018) 607-611.
27. X. Lv, J.G. Wu, J.G. Zhu, D.Q. Xiao, and X.X. Zhang, *J. Eur. Ceram. Soc.* 38[1] (2018) 85-94.
28. N.S. Zhao, H.Q. Fan, X.H. Ren, S. Gao, J.W. Ma, and Y.G. Shi, *Ceram. Int.* 44[1] (2018) 571-579.
29. H.R. Liu, P. Veber, J. Rödel, D. Rytz, P.B. Fabritchnyi, M.I. Afanasov, E.A. Patterson, T. Frömling, M. Maglione, and J. Koruza, *Acta Mater.* 148 (2018) 499-507.
30. X. Lv, J.G. Wu, J.G. Zhu, D.Q. Xiao, and X.X. Zhang, *J. Am. Ceram. Soc.* 101[9] (2018) 4084-4094.
31. X. Lv, N. Zhang, J.G. Wu, and X.X. Zhang, *Acta Mater.* 197 (2020) 224-234.
32. J. Yoo and S. Kang, *Crystals* 11[8] (2021) 859.
33. P.R. Ren, Z.C. Liu, M.Y. Wei, L.J. Liu, J. Shi, F.X. Yan, H.Q. Fan, and G.Y. Zhao, *J. Eur. Ceram. Soc.* 37[5] (2017) 2091-2097.
34. J.A. Sui, H.Q. Fan, B. Hu, and L. Ning, *Ceram. Int.* 44[15] (2018) 18054-18059.
35. K. Xu, J. Li, X. Lv, J.G. Wu, X.X. Zhang, D.Q. Xiao, and J.G. Zhu, *Adv. Mater.* 28[38] (2016) 8519-8523.
36. J.J. Ji, X. Li, B.J. Fang, X.Y. Zhao, S. Zhang, J.N. Ding, and H.S. Luo, *Ferroelectrics* 526[1] (2018) 33-45.
37. C. Wang, B.J. Fang, Y.H. Qu, Z.H. Chen, S. Zhang, and J.N. Ding, *J. Alloy. Compd.* 832 (2020) 153043.
38. C.Y. Shi, J. Ma, J. Wu, K. Chen, and B. Wu, *Ceram. Int.* 46[3] (2020) 2798-2804.
39. J. G. Wu, and Y. M. Wang, *Dalton Trans.* 43[34] (2014) 12836-12841.